

www.acsnano.org

In Situ Transmission Electron Microscopy Measurements of Ge Nanowire Synthesis with Liquid Metal Nanodroplets in Water

Quintin Cheek, $^\perp$ Eli Fahrenkrug, $^\perp$ Sofiya Hlynchuk, Daan Hein Alsem, Norman J. Salmon, and Stephen Maldonado*



Cite This: ACS Nano 2020, 14, 2869-2879



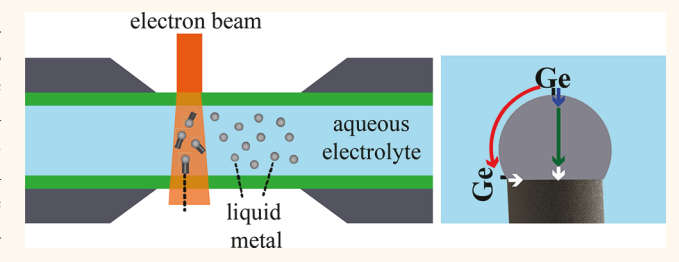
ACCESS

Metrics & More

Article Recommendations

Supporting Information

ABSTRACT: The growth of Ge nanowires in water inside a liquid transmission electron microscope (TEM) holder has been demonstrated at room temperature. Each nanowire growth event was stimulated by the incident electron beam on otherwise unsupported liquid Ga or liquid In nanodroplets. A variety of conditions were explored, including liquid metal nanodroplet surface condition, liquid metal nanodroplet size and density, formal concentration of dissolved GeO₂, and electron beam intensity. The cumulative observations from a



series of videos recorded during growth events suggested the following points. First, the conditions necessary for initiating nanowire growth at uncontacted liquid metal nanodroplets in a liquid TEM cell indicate the process was governed by solvated electrons generated from secondary electrons scattered by the liquid metal nanodroplets. The attained current densities were comparable to those achieved in conventional electrochemical liquid—liquid—solid (ec-LLS) growths outside of a TEM. Second, the surface condition of the liquid metal nanodroplets was quite influential on whether nanowire growth occurred and surface diffusion of Ge adatoms contributed to the rate of crystallization. Third, the Ge nanowire growth rates were limited by the feed rate of Ge to the crystal growth front rather than the rate of crystallization at the liquid metal/solid Ge interface. Estimates of an electrochemical current for the reduction of dissolved GeO₂ were nominally in line with currents used for Ge nanowire growth by ec-LLS outside of the TEM. Fourth, the Ge nanowire growths in the liquid TEM cell occurred far from thermodynamic equilibrium, with supersaturation values of 10⁴ prior to nucleation. These collective points provide insight on how to further control and improve Ge nanowire morphology and crystallographic quality by the ec-LLS method.

KEYWORDS: liquid TEM, in situ TEM, nanowire growth, nanocrystals, nanoparticle growth

roup IV semiconductor nanowires are attractive materials for current and emerging energy conversion, sensing, and electronic applications. ^{1–5} Irrespective of the target technology, the crystallographic and compositional attributes of Ge and Si nanowires are critical to their function and are determined during synthesis. Accordingly, a detailed understanding of the synthetic methods used to grow group IV semiconductor nanowires is key to realizing desired functionality.

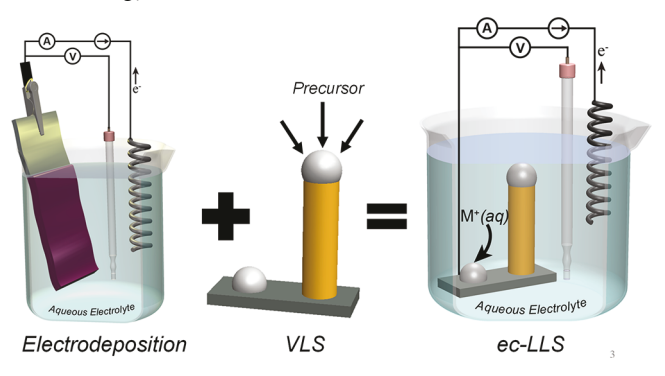
One nascent and potentially enabling synthesis method for crystalline Ge and Si nanowires is the electrochemical liquid—liquid—solid (ec-LLS) process. ^{6–8} In effect, this technique marries conventional electrodeposition with melt crystal growth by replacing the solid electrode with a liquid metal electrode. The crux of this technique is that the liquid metal serves as both a source of electrons and as a growth solvent for inorganic crystals, with the advantage that it can be performed at lower growth temperatures ($T < 100\,^{\circ}\mathrm{C}$) and ambient

atmosphere.⁹ Colloquially, ec-LLS is generally akin to performing vapor—liquid—solid (VLS)¹⁰ nanowire growth in a beaker and using electrochemistry rather than heat to drive the process (Scheme 1). To date, understanding of the ec-LLS process has come by way of indirect studies, for example, exhaustive analyses of as-grown materials^{5,11–13} or an indirect, ensemble spectroscopic measure of growth during an ec-LLS process.¹⁴ Detailed and direct insight on ec-LLS processes is presently lacking.

Received: August 14, 2019
Accepted: February 21, 2020
Published: February 21, 2020



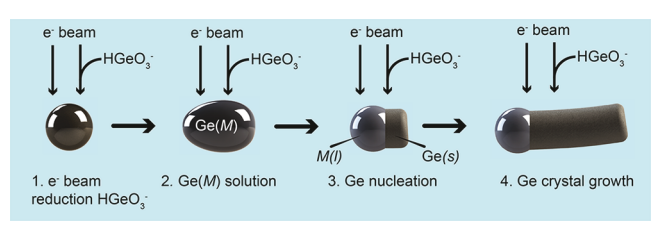
Scheme 1. Thematic and Simplified Description of the Growth of Crystalline Semiconductor Nanowires by the ec-LLS strategy^a



"The ec-LLS strategy combines the set-up and simplicity of conventional electrodeposition with the crystal growth metallurgy of VLS nanowire growth but without high temperatures or gaseous reactants. Notably, this depiction does not imply any specific mechanistic information regarding ec-LLS or VLS.

Recent advancements in analytical transmission electron microscopy (TEM) afford the possibility of studying nanomaterial growth processes with high fidelity. Specifically, with liquid TEM holders and fast-frame-rate digital detectors, it is possible to directly visualize discrete nucleation and nascent crystal growth events in solution with high spatial and temporal resolution. 15-21 In principle, an in situ TEM study of ec-LLS only requires housing a liquid metal volume(s) on a current collector within the viewing window of the liquid holder and then applying a potential/current to the liquid metal through the current collector. The metallurgical reactions between liquid metals and the majority of solid metal electrode materials substantially complicate this experimental design. However, in the course of performing such experiments, our lab observed a potentially simplifying phenomenon. Under certain experimental conditions, unsupported liquid metal nanodroplets could facilitate reduction of dissolved GeO2 and subsequent crystalline Ge nanowire growth simply by irradiation of the electron beam of the TEM (Scheme 2).

Scheme 2. Schematic Depiction of (1) an e⁻ Beam Causing the Reduction of Dissolved GeO₂ in Solution to Ge⁰, Followed by (2) Dissolution into a Liquid Metal Nanodroplet, Then (3) Crystal Nucleation, and Finally (4) Ge Nanowire Growth



This observation suggests that it may be possible to study ec-LLS events simply, *i.e.*, without a physical electrical contact or the use of an external current/potential source (*e.g.*, a potentiostat). In the context of ec-LLS growths of semiconductor nanowires, such measurements could prove valuable to answer several outstanding questions including: (1) is the growth rate of nanowires limited by chemical or electrochemical factors, (2) what are conditions necessary for nucleation and crystal growth, and (3) can the presence of crystallographic defects be minimized?

Herein, this report describes the phenomenon of unsupported liquid metal nanodroplets supporting covalent semiconductor nanowire growth in solution when irradiated by an electron beam. This study explores its utility as a streamlined approach for microscopic studies of semiconductor nanowire growth mediated by liquid metals. Specifically, liquid metal Ga and In nanodroplets are described here as potential platforms to initiate and study Ge nanowire ec-LLS in aqueous solution by the electrochemical reduction of dissolved GeO2. At this pH, the overall redox process can be described as $HGeO_3^- + 2H_2O + 4e^- \rightarrow Ge + 5OH^-$, since HGeO₃⁻ is the primary form of dissolved GeO₂. ²² Ga and In are important liquid metals because they are common constituents in most low-melting point metal alloys. 23,24 To date, these metals have been used extensively in ec-LLS studies since they afford the possibility of low-temperature semi-conductor nanowire syntheses. 12,25 This study tests three related hypotheses regarding these liquid metals. First, the use of the electron beam in liquid TEM experiments to induce nanowire growths specifically in the presence of liquid metals is general. Second, the nanowire growth rates are sensitive to the supply of electrons and affect the occurrence of crystallographic defects. Third, these nanowire growths occur under conditions far from equilibrium and have consequences on the resultant crystallinity. A series of micrographs and observations from in situ videos are presented below.

RESULTS AND DISCUSSION

Liquid Character of Metal Nanoparticles. The liquid TEM holder used in this work had no separate heating/temperature control. Accordingly, it was not clear *a priori* whether the metal particles studied here would be molten or solid. Two general observations were noted to ascertain liquid, rather than solid, character of the nanoparticles that are the focus of this work. If the metal particles coalesced rapidly, then liquid character was inferred, and/or if the particles yielded no definitive electron beam diffraction patterns, then liquid metal character was inferred.

Bulk Ga has a relatively low melting point $(T_{\rm m} = 29.8 \, ^{\circ}\text{C}).^{26}$ For Ga, fast coalescence of particles was routinely observed but only in solution (Figure 1a,b, accompanying Supporting Information, Video S2). In vacuum, Ga particles (both with ligands and those with a native oxide)²⁷ could be imaged in close proximity without any evidence of coalescence, even after focusing the electron beam to the highest possible density for prolonged periods. Presumably, the ligand and/or oxide shell prevented intermixing between two Ga droplets. In solution, Ga particles (even those on the micron scale) rapidly fused if they were being imaged while in close proximity with each other (Figure 1c). The short time scales of fusion provided compelling evidence of liquid character. The coalescence also implied that the local environment of the Ga droplets was strongly reducing, thereby removing/mitigating the native surface oxide. Separate measurements showed the native oxide of Ga could be electrochemically reduced at sufficiently negative potentials (Supporting Information, Figure S2). An alternative hypothesis for the fusion events could be that the electron beam generated vacancies/defects in the surface oxides via a knock-on displacement²⁸ from the incident electron beam (i.e., physical damage due to radiation

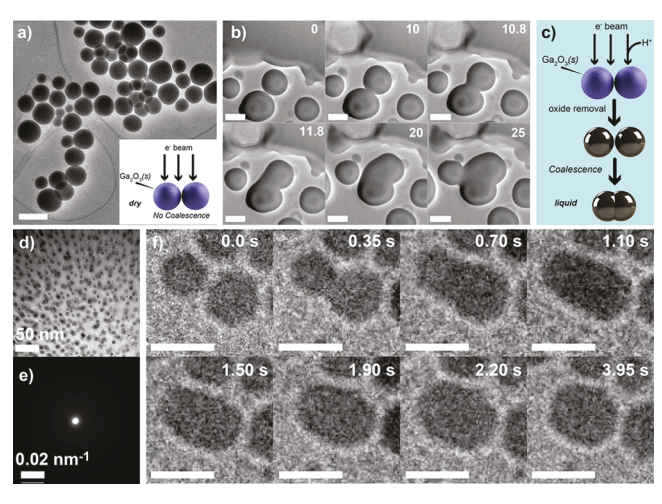


Figure 1. (a) Transmission electron micrograph under "dry" conditions of Ga nanodroplets coated with a native oxide. Scale bar: 1 μ m. Inset: Schematic illustration of how the native oxide of Ga droplets prevents coalescence. (b) Frame grabs from an *in situ* transmission electron microscopy video of Ga droplets immersed in an aqueous sodium tetraborate solution where the native oxide is unstable and coalescence occurs. Scale bar: 1 μ m. (c) Schematic depiction illustrating the removal of the native oxide on Ga nanodroplets under reducing conditions in solution. (d) Transmission electron micrograph of liquid In nanoparticles with radii \leq 10 nm. (e) Selected area electron diffraction collected from the same In nanoparticles in (d). (f) Frame grabs from an transmission electron microscopy video showing the coalescence between two In nanodroplets. Scale bar: 15 nm.

exposure). Although this scenario could not be ruled out, the likelihood that this would not occur in the dry state but would in the liquid environment seems low. Further, the reductive removal of the surface oxide is consistent with the further phenomenon reported below, while a knock-on mechanism is not. Finally, irrespective of how the surface oxide is ultimately removed by the electron beam, the rapid fusion of the droplets appears consistent with molten rather than solid metal character.

Separately, the melting point of bulk In is well above room temperature $(T_{\rm m} = 156.6\,^{\circ}{\rm C})$, ²⁹ but $T_{\rm m}$ for In nanoparticles can be greatly suppressed. Values as low as $T_{\rm m} = 25\,^{\circ}{\rm C}$ have been documented for In nanoparticles with radii (r) = 20nm.30 In nanoparticles on this size scale (Figure 1d) consistently did not exhibit any electron diffraction patterns when probed by selected area electron diffraction measurements (Figure 1e). For reference, In nanoparticles larger than this critical threshold regularly exhibited diffraction patterns consistent with solid, crystalline In in the liquid TEM holder. For In nanoparticles with $r \le 20$ nm, rapid coalescence of separate volumes into one was routinely observed. Figure 1f summarizes one such event, occurring within approximately 3 s (accompanying Supporting Information, Video S3). Similar events were observed to proceed in as little as 0.2 s (accompanying Supporting Information, Video S4). For reference, coalescence of similarly sized solid metal nanoparticles generally takes place over the course of tens of seconds. 31-33

General Observations of Ge Nanowire Growth *via* Electrochemical Reduction of Dissolved GeO₂ by the Electron Beam. Liquid metal nanodroplets facilitated nanowire growth when they were exposed to certain imaging

conditions in a medium that contained dissolved GeO₂ (as a precursor for Ge) and sodium tetraborate (to set the pH, to increase the solubility of GeO₂ in water, and to mirror the electrolyte of conventional ec-LLS). Energy dispersive X-ray spectra obtained on the nanowires confirmed they were composed of Ge (Supporting Information, Figure S4). When nanowire growth was observed, it generally occurred soon after first exposure to the electron beam. Just prior to the emergence of an obvious nanowire crystal, the apparent radius of the liquid nanodroplets increased (vide supra). During these experiments an objective aperture was used to enhance contrast and to allow for sufficient beam current to reduce oxidized Ge in solution.

Five parameters were noted as particularly influential regarding whether a nanowire growth event occurred. First, precipitation/nucleation/crystal growth of Ge⁰ did not occur in the absence of liquid metal nanodroplets. Prolonged imaging of solutions containing only dissolved GeO2 and sodium tetraborate but without metal nanoparticles never yielded any spontaneous reduction of GeO₂. That is, the incident imaging beam was insufficient under any attainable imaging condition to drive zerovalent Ge formation. This point stands in contrast to simple metal salt reduction, which was both observed in this work and has been documented extensively by several laboratories. 17,34,35 Second, the presence of surface ligands on the liquid metal nanodroplets was important. Liquid metal nanodroplets without any capping ligands were prone to rapid dissolution upon imaging (vide infra). However, when an excess ligand concentration was used during synthesis of the liquid metal nanodroplet that saturated the surface adsorbed ligands, the liquid metal nanoparticles were indefinitely stable but never supported nanowire growth. Ge nanowires were only grown from liquid metal nanodroplets that possessed an intermediate ligand coverage. Third, we observed that Ge nanowire growth was not possible at all formal concentrations of dissolved GeO₂. For formal GeO₂ concentrations <5 mM, no Ge nanowire growth events were ever observed. Prolonged imaging of liquid metal nanodroplets (>60 s) in these solutions under any imaging condition only resulted in the nucleation of (presumably) an $H_2(g)$ bubble. However, above this threshold formal concentration of dissolved GeO2, Ge nanowire growth was routinely possible. The upper limit on the formal concentration of GeO₂ was limited to 100 mM, as GeO₂ precipitates and clogs the lines above this value, even if the bulk solutions were sufficiently metastable for conventional Ge ec-LLS on the benchtop. Fourth, a threshold for the electron beam current density was required to induce and drive nanowire growth at liquid metal nanodroplets. The electron beam density was adjusted in one of two ways: either the absolute current of the electron beam was manually varied or the beam diameter was adjusted by controlling the condenser lens current. An approximate estimate of the threshold electron beam current density was 8 nA μ m⁻² (800 mA cm⁻²). This current corresponded to a dose rate of $\sim 4 \times 10^9$ Gy s⁻¹. Fifth, the areal density of liquid metal nanodroplets was strongly influential on whether ec-LLS was observed. Isolated (≤1 per μ m⁻²) liquid metal nanodroplets never yielded Ge nanowires. Lastly, Ge nanowires were also observed in regions of the liquid TEM cell that were not directly imaged but were just proximal (within a few hundred nm) to irradiated areas.

Ge Nanowire Growth with Ga Nanodroplets. Using the conditions amenable for electron-beam-induced nanowire growth, the growths of multiple Ge nanowires facilitated by

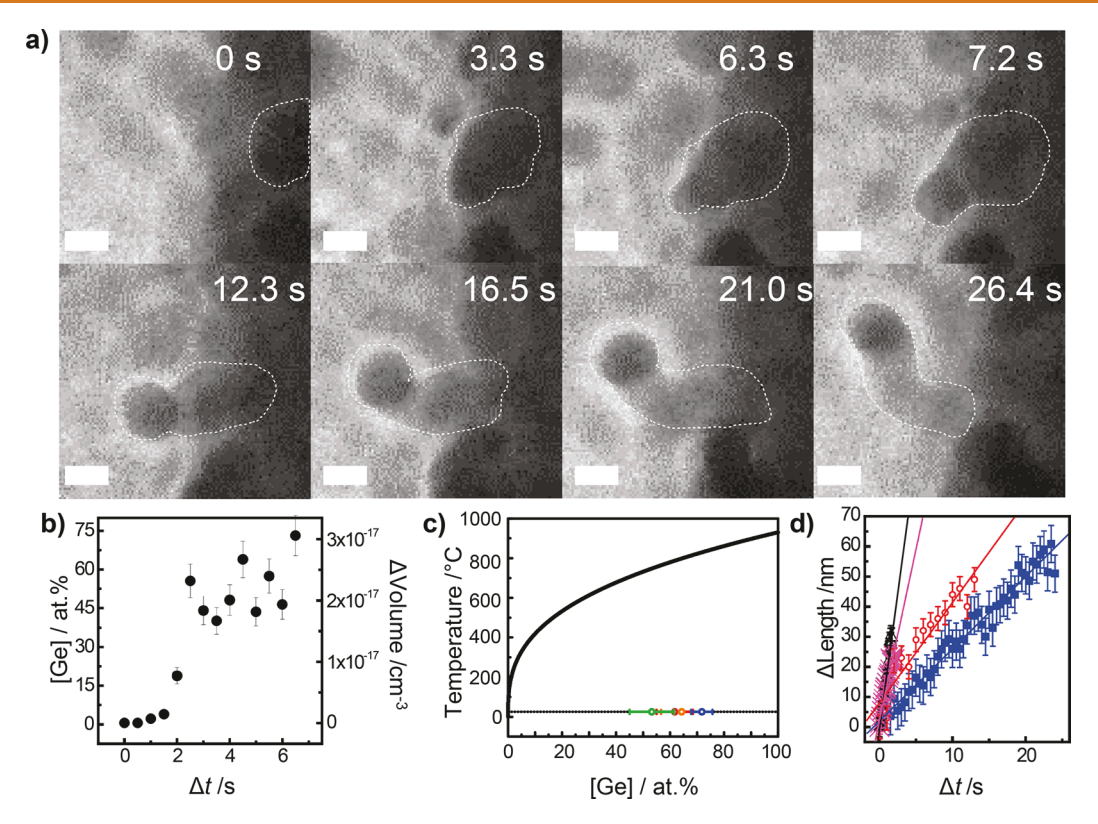
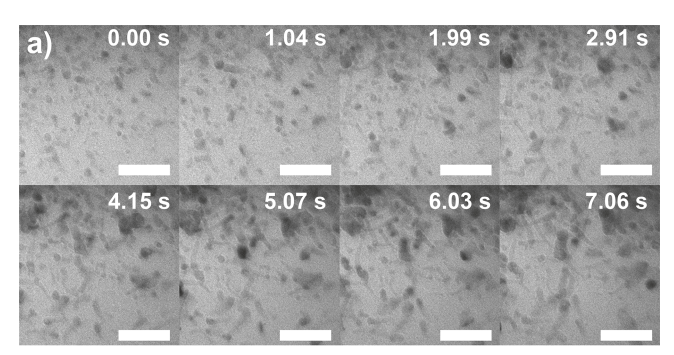


Figure 2. (a) Frame grabs from an *in situ* transmission electron microscopy video of a Ge ec-LLS event with a Ga nanodroplet immersed in an aqueous solution containing dissolved 0.05 M GeO₂. Scale bar: 50 nm. (b) A plot showing the volume change of the Ga nanodroplet as a function of time before Ge nucleation occurred. (c) The phase diagram for the Ga—Ge system is shown with the inclusion of data from four different Ge nanowire growth events. The colored data points correspond to the inferred Ge concentration in the Ga nanodroplets at the time just before nucleation. (d) A plot of Ge nanowire length *vs* time for four separate Ge nanowire growth events. The steady-state growth rates were estimated from the linear-least-squares fitting of the data (red lines).

Ga nanodroplets were observed. Figure 2a shows frames from a representative video showing the initial stages of a Ge nanowire growth from a Ga nanodroplet (Supporting Information, Video S5), with a corresponding plot of the volume change vs time (Figure 2b) that occurred prior to the emergence of a Ge nanowire. The estimated concentration of Ge in the Ga nanodroplet inferred from the volume change (assuming ideal behavior for the liquid Ga-Ge solution) for four different events was 63 ± 14 at. %. This value corresponds to a supersaturation of Ge in Ga reaching ~10⁴, assuming the equilibrium solubility of Ge in Ga is 0.0045 at. % at T=25°C.³⁶ For reference, the individual supersaturation values in at. % from four Ge nanowire growths are superimposed on the Ge-Ga phase diagram³⁷ in Figure 2c. These data show that these ec-LLS Ge nanowire growths occurred at a temperature well below the thermodynamic melting temperature of the Geliquid metal mixture, as indicated on the phase diagram. Figure 2d shows four separate plots of Ge nanowire lengths vs time for four separate ec-LLS events measured in four separate cells, that is, not at the same time. A monotonic trend was observed in all cases, indicating a steady-state nanowire growth. Using the slope of the best-fit line for each growth as the average growth rate, the observed growth rates ranged from 2.4 ± 0.1 to 18 ± 6 nm s⁻¹. Across these four measurements, it was not possible to directly ascribe the differences in growth rates solely to one variable, as differences in liquid solution thicknesses, electron beam stability, and type of detection camera varied between experiments performed on different imaging sessions. Nevertheless, these growth rates were

consistent with a prior report of nanowire growth featuring solute trapping. Based on the growth rates and diameters of these nanowires, the average faradaic current densities attained during these nanowire growths (assuming an overall $4e^-$ redox process and the nanodroplet operates as a hemispherical ultramicroelectrode) ranged from 3.4 ± 0.1 to 25.5 ± 0.9 mA cm⁻².

Ge Nanowire Growth with In Nanodroplets. In nanodroplets proved similarly capable of sustaining Ge nanowire growth. Anecdotally, for the same experimental conditions, initiating and viewing nanowire nucleation and growth with In nanodroplets proved significantly more facile than with Ga nanodroplets. Figure 3a shows frames from a representative movie of nanowire growth occurring at several In nanodroplets within the field of view (Supporting Information, Video S6). The time stamps in this figure and all other frames are relative, as the area was irradiated by the electron beam momentarily while area was being selected for imaging. Figure 3b highlights the growth of a single Ge nanowire over less than 3 s (accompanying Supporting Information, Video S7). This movie encapsulates several relevant points. First, capturing cleanly the initial nucleation for each nanowire was not always possible. In this movie, the Ge nanowire had already grown as a partial coil, as is evident in the first frame. Second, the growth direction of individual nanowires often changed. Third, even at high magnification, the image resolution was limited by scattering from water, obscuring lattice fringes.



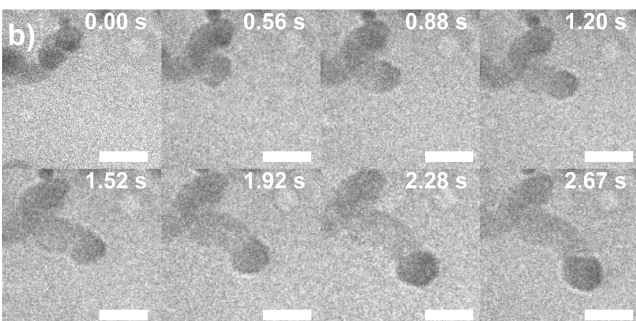
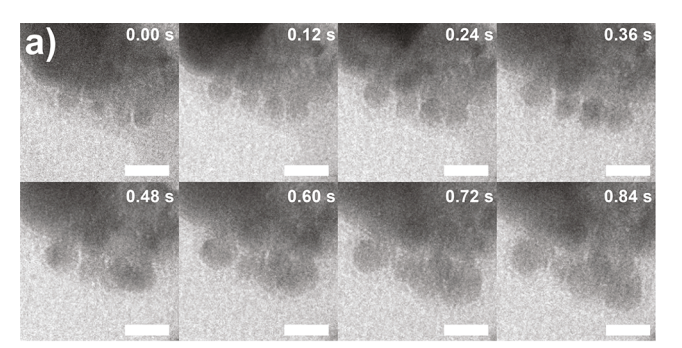


Figure 3. (a) Frame grabs from an *in situ* transmission electron microscopy video of parallel Ge nanowire growth events at In nanodroplets immersed in aqueous solution with a formal GeO_2 concentration of 0.05 M. Scale bar: 20 nm. (b) Frame grabs from an *in situ* transmission electron microscopy video of a single Ge nanowire growth event in an aqueous solution with a formal GeO_2 concentration of 0.05 M. Scale bar: 75 nm.

Figure 4a highlights the short time period for a set of adjoining In nanodroplets prior to nucleation and growth of Ge nanowires (Supporting Information, Video S8). In these images, the volume of the In nanodroplet increases quickly without obvious Ge nucleation. Due to the limited resolution of imaging in liquids and the crowding in these images, the unambiguous observation of volume swelling prior to the start of every Ge nanowire growth was not possible. Still, Figure 4b shows the relative volume changes over time up to the point of nucleation for 5 different nanowires. Assuming these volume changes corresponded to concentrations of Ge in the liquid metal nanodroplets at the time nucleation, these data implicated an average Ge concentration in liquid In of 80 ± 13 at. %. For reference, the equilibrium solubility of Ge in In is 0.00075 at. % at T = 25 °C.³⁶ However, the specific supersaturation value of Ge in In is ambiguous, as the Ge-In solubility value rigorously holds only for dissolved Ge in bulk, solid In. Still, these observations generally imply a similarly large, $\sim 10^4$ supersaturation of Ge in In.

Figure 5 shows representative Ge nanowire length ν s time plots, again highlighting monotonic growths with respect to time. Since the propensity for Ge nanowire growth with In nanodroplets was high, it was possible to collect these data simultaneously, that is, under the same imaging conditions. Accordingly, Figure 5b shows a plot of the observed growth rates as a function of the nanodroplet radius. A clear trend was observed, with the apparent growth rate decreasing as the nanodroplet radius increased. Based on the growth rates and radii of the nanodroplets, an average faradaic current density for these wire growths was estimated, ranging between 12 and 23 mA cm⁻². For reference, the mass-transport-limited current for hemispherical ultramicroelectrodes in this size range (=



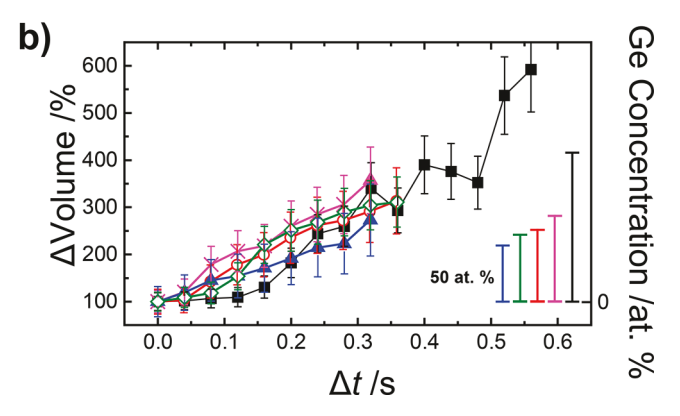


Figure 4. (a) Frame grabs from an *in situ* transmission electron microscopy video depicting the volume change demonstrated by four In nanodroplets due to the incorporation of Ge from the beam-induced reduction of dissolved ${\rm GeO_2}$. Scale bar: 20 nm. (b) A plot illustrating the volume change in five separate In nanodroplets over the time prior to Ge nucleation. The right axes scale is different for each nanodroplet since the radius varied across this set of five.

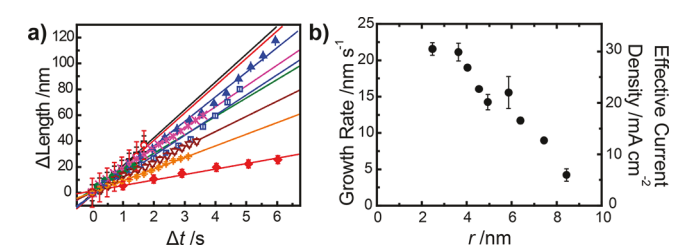


Figure 5. (a) A plot of Ge nanowire length vs time for 9 different Ge nanowire growth events at different In nanodroplets imaged under the same conditions. The steady-state growth rates were estimated from the linear-least-squares fitting of the data (color-coated solid lines). (b) A plot of the estimated nanowire growth rate in (a) as a function of the In nanodroplet radius.

 $2nFD[\text{GeO}_2]\pi^{-1}r^{-1}$, where n is the number of electrons involved, F is Faraday's constant, $[\text{GeO}_2]$ is the concentration of reducible dissolved GeO_2 , and D is the diffusivity of redox species) in a quiescent solution would be >10,000 mA cm⁻².

Figure 6 highlights two additional interesting phenomena. First, the growth rate tracked directly with the electron beam intensity. Frames from a video of an experiment where the Ge nanowire growth process was modulated by adjusting the electron beam intensity are shown in Figure 6a (Supporting Information, Video S9). In these panels, the electron beam intensity was increased by a factor of 3.5 at $t=2.25\,\mathrm{s}$ by adjusting the condenser lens current to change the diameter of the electron beam while the nanowire growth was continuously imaged. The corresponding growth rate plot is shown in Figure

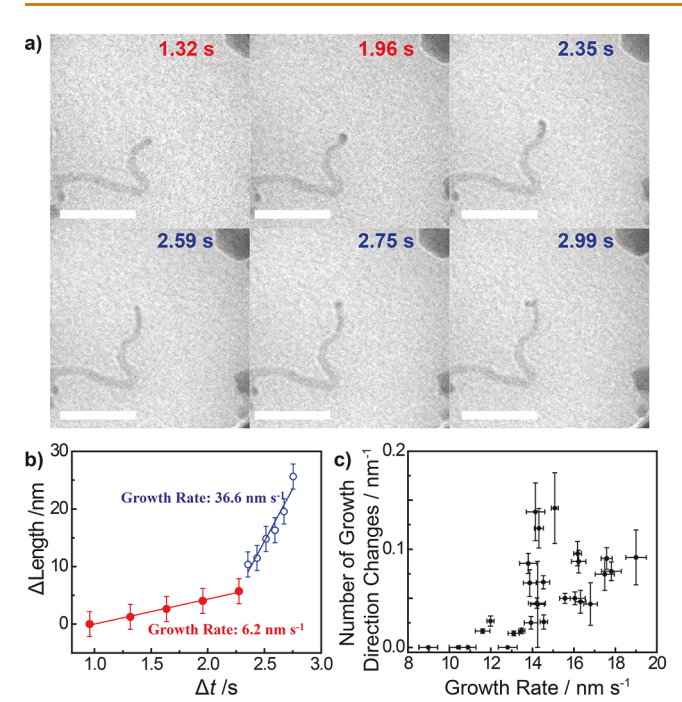


Figure 6. (a) Frame grabs from an transmission electron microscopy video illustrating the growth of an individual Ge nanowire as a function of the electron beam intensity. The top three frames were recorded during a "broad" beam condition, while the bottom three frames were collected during a "focused" beam condition. Scale bar: 50 nm. (b) A plot of the nanowire length vs time for the nanowire in (a). The red solid circles correspond to measurements under the "broad" beam condition. The open blue circles correspond to measurements under the "focused" beam condition. (c) A plot of the number of observable growth direction changes for Ge nanowires as a function of the observed steady-state growth rate.

6b. When the electron beam intensity was increased, the apparent growth rate accelerated by a factor of 6. Second, the number of changes in nanowire growth direction rose after the growth rate increased. To ascertain explicitly whether there was a correlation, a series of Ge nanowire growth events (N=30) were analyzed in detail. Figure 6c shows that the propensity for growth direction changes (normalized by final nanowire length) generally tracked with faster nanowire growth rates. To be clear, only "lateral" growth direction changes were observable by this mode of imaging. Nevertheless, although the correlation was not strictly monotonic, nanowires grown at faster rates generally were much less straight.

Global Interpretation of the Cumulative Data. The data in this work support several important points. First, the observation of a spontaneous reduction of dissolved GeO₂ at liquid metal nanodroplets in a liquid TEM cell is in fact an electrochemical process without an external supply source like a potentiostat. Accordingly, these events can properly be described as ec-LLS. Second, the conditions necessary for initiating ec-LLS at uncontacted liquid metal nanodroplets in a liquid TEM cell highlight necessary factors for Ge ec-LLS to occur. Third, the nanowire growth rates reported here are in line with previous reports and suggest that crystal growth is limited by the feed rate of Ge into the liquid metal rather than the rate of crystallization. Fourth, nanowire growth in ec-LLS

occurs far from thermodynamic equilibrium, impacting nanowire morphology and crystallographic quality.

Stimulated ec-LLS by the Incident Electron Beam. One possible interpretation of the observed Ge nanowire growths is that the phenomena were more akin to a chemical, solution—liquid—solid^{39,40} process that was thermally driven by the electron beam rather than electrochemical in nature. This interpretation is negated in the following ways. First, the temperature change in aqueous solutions induced by the incident electron beam in liquid TEM experiments has been proven to be small,³⁴ on the order of ~4 °C. Ge nanowire growth is not possible just by heating (to much larger temperatures approaching the boiling point of water) in solutions containing dissolved GeO₂, supporting electrolyte, and liquid metals are well established. 5,6,9,12,13,25 Second, any heating of the solution by the electron beam would not strongly depend either on the density of nanodroplets in solution or the concentration of dissolved GeO₂. However, both aspects were observed to definitively influence the propensity for nanowire growth.

Although there are similarities to two separate types of phenomena, the data shown here are unlike anything ever reported in the in situ liquid TEM literature. Certainly the precedent for the electron beam in liquid TEM experiments to induce electrochemical reduction of species dissolved in solution is well established. 35,41-45 In fact, this premise was explicitly used here to generate liquid Ga and In nanodroplets directly in the liquid holder cell. However, this work makes clear that direct irradiation (i.e., imaging) of the GeO₂ solution is insufficient to nucleate any solids, implicating that it is not possible to generate stable Ge nuclei in water solely by radiolytic species or solvated electrons generated by the electron beam passing through water and the SiN windows. Rather, the presence of a liquid metal nanodroplet is a necessary criterion to locate and facilitate Ge nucleation and crystal growth. In this regard, the work presented here stands apart from electron-beam induced metal electrodeposition works 16,35,42 and instead has parallels to in situ TEM semiconductor nanowire growths by the VLS process. 46-48 The volume swelling of the liquid metal prior to observing nanowire growth further supports this interpretation, which is fully in line with the current understanding of nanowire growths catalyzed by liquid metal nandroplets. 25,49,5

Questions remain as to how exactly how the electron beam instigates the electrochemical reduction of dissolved GeO₂. One hypothesis is that the liquid metal nanodroplets are charged by the incident electron beam, effectively shifting their potential to more negative values where eventually the reduction of dissolved GeO2 is thermodynamically spontaneous. This interpretation has two unresolvable complications. First, it implies that the principle of charge neutrality in solution is violated, as no corresponding oxidation reaction would be required. Second, it suggests that imaging any metal electrode by an incident electron beam would always shift unabated its potential to progressively more negative potentials. This scenario has not been observed previously. In fact, we previously noted any shifts of an electrode's potential induced by the electron beam were small, timeindependent, and depended heavily on the specific experimental design.⁵¹

A second hypothesis is that the solvated electrons generated by the primary electrons of the incident electron beam are the reductants that react with dissolved GeO_2 . This contention

suggests that the density of available reductants (solvated electrons) would then be solely dependent on the intensity of the electron beam in the solution, implying the growth of Ge nanowires would occur even at a single, isolated liquid metal nanodroplet. The observations presented above are counter to this premise.

A third hypothesis more in line with the cumulative observations is that the reductants are solvated electrons generated by secondary electrons scattered primarily from liquid metal nanodroplets. All materials irradiated by the electron beam (i.e., windows, solution, nanodroplets) release secondary electrons through scattering events with the primary beam. 44,5 These secondary electrons have an extremely short-range (~5-10 nm)^{53,54} but are capable of generating solvated electrons that can reduce species in solution. 41,43,55 The inferred faradaic current for GeO2 reduction is roughly 2.5% of the incident primary electron beam density, a value roughly in agreement for the steady-state yield of secondary electron processes.⁵⁵ A higher areal density of irradiated objects (e.g. cluster of liquid metal nanodroplets) would correspondingly lead to a higher steady-state concentration of solvated electrons from secondary electrons. Conversely, when irradiated objects are not concentrated or totally isolated, the number of secondary electrons available to generate solvated electrons to drive reduction of GeO2 would be correspondingly small. These aspects are in line with the observation that Ge nanowire growth events were much more probable with higher densities of liquid metal nanodroplets. Further, this hypothesis could also help explain (in part) why the probability of observing Ge nanowire growths was anecdotally higher with In rather than Ga nanodroplets. The coefficient for secondary electron emission, δ , is generally larger for elements with larger atomic number. 56 For Ga and In specifically, the δ value is ~35% greater for In than for Ga. 56 Based on these points, we posit that the Ge nanowire growths shown here were dictated largely or exclusively by solvated electrons generated from secondary electron scattering.

To be clear, the designation of "ec-LLS" for the nanowire growth events shown here should not be confused with any colloquial meaning of the term 'electrochemistry'. By no means was an external power supply or potentiostat used to drive the reduction of dissolved GeO₂ that necessarily occurred here. Further, we do not discount the occurrence of radiolytic reactions in the solution, as are known to occur in liquid TEM experiments. 55 Rather, we simply feel the data are clear that the chemical phenomena involved in Ge nanowire formation are unambiguously induced by and tied to the electrostatic influence of the incident electron beam. Accordingly, the designation of these data as "electrochemical" reflects this point. The connection to "ec-LLS" is also clear since the nanowire growths are necessarily dependent on the presence of liquid metal nanodroplets. Hence, we feel the results shown here provide significant insight on ec-LLS processes outside of the TEM.

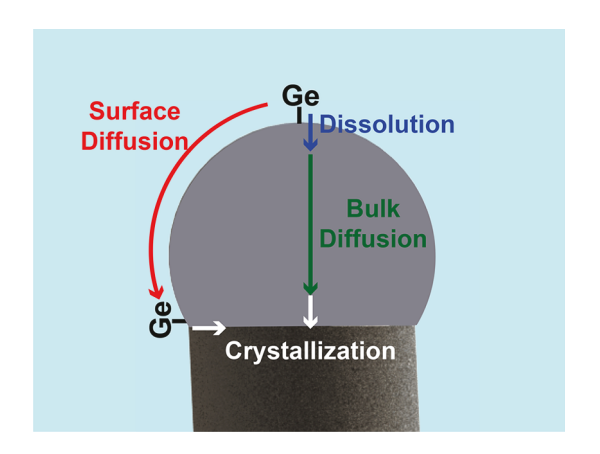
Surface Condition of Liquid Metal Nanodroplets for Ge Nanowire Growth. Three notable observations indicated the surface of the liquid metal nanodroplets is a more important factor than previously considered. The total absence of an observable volume change in the liquid metal nanodroplets in dilute (<5 mM) solutions of dissolved GeO₂ implied the flux of Ge⁰ into the liquid metal nanodroplets was effectively zero. This point suggests that the formal concentration in solution did not directly relate to the rate

of reduction (as would be expected for the reduction of a diffusion limited species in solution). Prior electrochemical studies of Ge ec-LLS on Hg microdroplets support a complicated mechanism for the reduction of ${\rm GeO_2}$ where adsorbed species may be involved. ⁵⁷ If a rate-determining intermediate is surface bound and at too low of a surface coverage to result in the formation and dissolution of ${\rm Ge^0}$ into the liquid metal, then Ge nanowire growth will not occur. The role of at least one surface-bound species in the electrochemical process is further in line with separate observation that Ge nanowire growth was never observed when the liquid metals were exposed to saturating levels of citrate ligands. Previous studies on ec-LLS presumed the surface of the liquid metal just needed to be oxide-free to crystal growth. ^{12,25}

A third, separate observation that speaks to the role of surface conditions is the decrease of the growth rate as the nanodroplet radius increases. The general characteristic for VLS-based nano/microwire growths is that nanowire growth rates typically increase with increasing metal droplet radii up to a saturating growth rate for the specific reaction conditions.⁵⁸ An inverse correlation where nanowires grow slower at larger nanodroplet sizes has been observed experimentally 59,60 and predicted theoretically 61-64 but generally only applies under certain conditions. Specifically, when the incorporation of solute (Ge) into the volume of the liquid metal is slow enough that another process (e.g. surface diffusion) can augment the delivery of solute to the liquid metal/solid crystallite interface, then an inverse growth rate-radius correlation will be operative. For VLS growths in molecular beam epitaxy systems, adatom diffusion occurs from the substrate and nanowire side to the crystal growth front at the liquid metal/nanowire interface.65 In the results presented here, neither possibility is viable since Ge is electrocatalytically inactive for GeO2 reduction. Instead, we argue the possibility that an adlayer of Ge⁰ remains at the liquid metal/liquid electrolyte interface that could diffuse on the surface of the liquid metal nanodroplet without having to dissolve within the bulk liquid metal volume. If these species reach the liquid metal/nanowire interface, they ought to be able to participate in crystallization. Scheme 3 summarizes this point.

Crystal Growth Rates in Ge Nanowire ec-LLS. In principle, the electron beam intensity afforded the possibility of controlling nanowire growths in the same manner that an

Scheme 3. Schematic Depiction of Ge⁰ Transport Both through the Liquid Metal Bulk (as Solute) and Across the Surface (as Adsorbate) to the Crystal Growth Front



applied current does in a traditional electrodeposition experiment. The requirements for imaging and the propensity for generating H₂ bubbles set the lower and upper bounds on the usable electron beam intensity. Still, over the limited available range, the fact that the constant growth rates could be modulated directly by the electron beam intensity at effective current densities well below the mass transport limit indicates that the rate of nanowire growth was likely kinetically limited by the electrochemical reduction reactions of dissolved GeO₂. If the kinetics of electroreduction were sufficiently fast that mass-transport of dissolved GeO2 by radial diffusion to the liquid metal interface was instead controlling, then the nanowire growth rates would have been much faster, insensitive to the electron beam intensity, and instead directly dependent on the concentration of dissolved GeO2. Those aspects were not observed here. Ge nanowire growth rates limited by the kinetics of the electroreduction reaction also necessarily mean that the rate of crystallization inside the liquid metal nanodroplets was faster. Accordingly, the crystal growth rates for the events detailed here must be >10⁻⁸ m s⁻¹

The reason why Ge crystallization rates can be large in ec-LLS with Ga and In is not immediately clear but the data point to one likely possibility. For both Ga and In, ec-LLS occurred under extremely high supersaturations of Ge in the liquid metals on the order of 10⁴, representing extremely large driving forces for crystallization. The reason why such large Ge supersaturations were attained is less obvious, as it implies that a sizable activation barrier for nucleation exists in these systems. A similar inference of a large activation for Ge nucleation in Ga was noted previously in Ge microwire ec-LLS, 14 although in that work the supersaturation values were more than an order of magnitude lower. It is not clear whether the difference arises from the sensitivities of the employed methods, the lack of an underlying solid substrate as compared to the traditional electrochemical experiments, or the difference in liquid metal sizes. Nevertheless, the fact that large supersaturation values were observed in two distinct liquid metals suggest this activation barrier may be a general feature of low-temperature Ge crystal growth. Future studies with other liquid metal nanodroplets (e.g. Hg, In-Bi) would be informative on this point.

A consequence of fast crystal growth rates is the greater likelihood of crystallographic imperfections. The data here support this point. It is not clear what specific crystallographic defect type(s) were responsible for the growth direction changes (e.g., substitutional defects like liquid metal inclusions and lattice substitutions or twin dislocations). Nevertheless, the data strongly suggest that one pathway to straighter nanowires with fewer crystallographic defects is to slow down the nanowire growth. In principle, this can be achieved by adjusting applied potentials/currents (in conventional ec-LLS) or the flux of irradiation (as shown here) but not necessarily by lowering the concentration of GeO_2 in the electrolyte.

CONCLUSION

The work presented here introduces and outlines a viable methodology for studying crystalline nanomaterial growth by ec-LLS. This approach affords insight on the elementary processes involved in this hybrid electrochemical/metallurgical materials synthetic method. Doing so has highlighted that ec-LLS occurs under conditions where the rate of heterogeneous reduction of dissolved GeO₂ limits nanowire growth rather than the rate of crystallization. The measured supersaturations

are surprisingly large, indicating a high activation barrier for nucleation that seems to be similar for two dissimilar liquid metals. Additionally, the data shown here suggest further studies to characterize the nature of the liquid metal/ electrolyte interface in more detail are warranted. In a larger sense, these data also suggest it might be possible to perform similar "wireless" ec-LLS nanowire growths by a bulk radiolysis technique that also generates solvated electrons. 67,68 In this way, it may be possible to further extend ec-LLS toward conditions that more closely mirror solution-liquid-solid nanowire syntheses⁴⁰ but with simpler, oxidized reagents that can be reduced electrochemically. Additionally, the prevalence of surface- rather than bulk-diffusion processes as controlling the observed nanowire growth suggests the possibility of using larger solid particles. The prospects for this type of growth will be detailed in a follow up report.

METHODS

Materials. Germanium(IV) oxide (99.999%, Alfa Aesar), indium(III) bromide (99.99%, Acros Organics), indium(III) chloride (99.99%, Acros Organics), gallium(III) nitrate (99.9998%, Acros Organics), disodium citrate hydrate (>99%, Fischer Scientific), potassium nitrate (99+%, Acros Organics), gallium tris-(dimethylamide) dimer ($Ga_2(NMe_2)_6$, (99.9% ampouled under argon, Alfa Aesar), sodium borohydride (98%, Spectrum), di-noctylamine (≥97.0%, Sigma-Aldrich), 1-octadecene (≥95.0%, Sigma-Aldrich), sodium tetraborate (>99.5% Sigma-Aldrich), and oleic acid (90% technical grade, Sigma-Aldrich) were used as received. $Ga_2(NMe_2)_6$ was stored in the glovebox prior to use. InCl₃, InBr₃, and $Ga(NO_3)_3$ were stored in a desiccator prior to use. Water with a resistivity >18.2 $M\Omega$ -cm (Nanopure Barnstead Water Purification) was used throughout.

Electron Microscope. All TEM experiments were performed in a JEOL 2010F field emission analytical microscope operated at an acceleration voltage of 200 kV in parallel beam (TEM) mode. Images were collected without insertion of condenser or intermediate lens apertures. However, an objective aperture was used to enhance contrast during imaging. Still images and videos were collected with either a Gatan 794 Multiscan camera at 3 frames per second with a pixel resolution of 1024 × 1024 or a Gatan One View camera at 4k (25 frames per second) or at 2k (100 frames per second) pixel resolution.

Liquid Cell TEM Apparatus. Experiments were conducted with a commercial liquid TEM sample holder and microfabricated Si chips from Hummingbird Scientific (Lacey, WA). The general configuration relies on a thin nanofluidic channel formed by compressing and sealing two microfabricated Si chip sets (\sim 50 nm SiN $_x$ window, spacer thickness of 250 nm, cell volume = 7.69×10^{-6} cm³, window area = 1.95×10^{-4} cm²) into the tip of a custom TEM sample holder. Prior to use, each Si chip set was plasma etched with Ar(g) for 2 min to clean and render hydrophilic interfaces. Following assembly of the liquid cell, the holder was inserted into a secondary evacuated cell held at 8×10^{-6} Torr for 15 min to ensure mechanical stability of the liquid cell prior to insertion into the TEM. Prior to each experiment, solution was flowed into the chip set through plastic tubing via a programmable syringe pump at a constant flow rate. During imaging, this flow rate was held constant at 5 μ L min⁻¹. Following each experiment, the lines to the liquid TEM cell were rinsed with pure H_2O at a rate of 15 μ L min⁻¹ for 20 min to avoid cross contamination between experiments.

Ex Situ Gallium Nanodroplet Synthesis. Gallium nanodroplets that were prepared outside of the TEM were synthesized by a hot injection method from dried reagents using a synthetic procedure under an inert atmosphere previously reported for synthesis of ~60 nm particles. Fig. 1-octadecene (7 mL) was added to a three-neck round-bottom flask equipped with a condenser and then stirred magnetically under argon. The solution was heated to 280 °C. A solution of 25 mg gallium tris(dimethylamide) in di-n-octylamine

(3.39 mL) and 1-octadecene (2.61 mL) was injected into the hot reaction flask. The solution color changed from yellow to dark gray within 60 s. The reaction flask was removed from the heating mantle and cooled to room temperature with a computer fan and an ice bath. Chloroform (10 mL), oleic acid (1 mL), and ethanol (20 mL) were added to clean the contents of the round-bottom flask. Centrifugation was performed at 6000 rpm for 10 min and then repeated a total of three times for Ga nanoparticle isolation. For storage purposes, the nanoparticles were dispersed in an ethanol solution. For dry TEM imaging, the colloidal solution was drop-cast directly on a TEM grid. For liquid cell experiments, a solvent exchange process was carried out. First, 5 mL of the ethanol solution was centrifuged for 10 min at 6000 rpm. The ethanol was exchanged with water and resuspended. This process was repeated twice. On the third time, an aqueous solution of 50 mM GeO₂ and 10 mM Na₂B₄O₇ was used to exchange the pure water.

Ex Situ Indium Nanodroplet Synthesis. Indium nanodroplets were prepared by a one-pot synthesis method that was previously reported for allowing the synthesis of In spheres with a diameter ranging from 10 to 100 nm. 15 mL of diethylene glycol solvent was added to a three-neck round-bottom flask containing 1.6 mg InCl₃ and 2.1 mg disodium citrate hydrate. The flask was then purged with Ar(g) for 30 min, followed by heating to 100 °C. 2.7 mg NaBH₄ was then dissolved in 1.0 mL of water. After the solution remained at 100 °C for 10 min, the NaBH₄ solution was injected into the round-bottom flask, resulting in an immediate color change. These nanodroplets were then separated and prepared for analysis in the same manner described above.

In Situ Synthesis of Liquid Metal Nanodroplets. Metal nanodroplets were also synthesized directly inside the liquid TEM holder cell through reduction of a dissolved metal salt by the imaging electron beam. Generally, these solutions contained 10 mM metal salt (InBr₃ or $Ga(NO_3)_3$), 10 mM disodium citrate hydrate, and 100 mM KNO₃ and were injected into the liquid cell at a rate of 5 μ L min⁻¹ for 5 min to flush the cell entirely with this solution. The holder was then inserted into the TEM for imaging. Under high-intensity imaging conditions, metal nuclei were routinely observed. In the absence of any added citrate in solution, the metal nanodroplets were unstable after formation, regularly dissolving away after prolonged beam exposure (accompanying Supporting Information, Video S1).

In Situ Ge Nanowire ec-LLS. A solution containing 50 mM ${\rm GeO}_2$ and 10 mM sodium tetraborate was then injected at a rate of 5 μ L ${\rm min}^{-1}$ for 15 min to flush three dead volumes. Even after flushing the cell for 15 min, a large number of liquid metal nanodroplets remained on or near the window of the cell. During these experiments, the condenser lens current was adjusted so that the beam size was approximately equal to the field of view in each movie, that is, the center to the corner of the field of view was approximately equal to the radius of the beam. An objective aperture was used to enhance contrast and a selected area aperture for diffraction, but otherwise no apertures were used.

Data Analysis. All image analysis was performed using FIJI (Ver 1.52p). Two methods were employed for tracking the growth rates of nanowires in these studies. If there was no sample drift present in the data frames, then the length of the wire was tracked by placing a tick at the front of the liquid metal cap for each frame. Then, the position of each tick was measured in FIJI allowing for the distance between each tick to be calculated and summed to retrieve the length of the nanowire at each point in time. If significant drift was present, then the nanowires lengths were measured manually for each frame using the segmented line tool in FIJI. These nanowires lengths were then plotted vs time allowing for a growth rate to be determined from the slope of the line of best fit. The time zero points in most of the movies collected for data analysis represent the first instant after the position of the beam was set and the beam was unblanked to initiate imaging. However, in some occasions, the beam was unblanked, nanowire events were observed, and then the beam was repositioned to better view additional events. Accordingly, in these movies, the time stamps are referenced to an arbitrary start time. In order to determine the supersaturation of Ge in the liquid metal nanodroplets, the diameters

of the nanodroplets were measured using the line tool in FIJI at each point in time. Assuming each nanodroplet was a perfect sphere, the volume of the nanodroplet was calculated based on the diameter measurement at each point in time. Changes in volume were interpreted as changes in liquid metal composition by dissolution of Ge into the liquid metal.⁴⁹

ASSOCIATED CONTENT

Solution Supporting Information

The Supporting Information is available free of charge at https://pubs.acs.org/doi/10.1021/acsnano.9b06468.

Additional details including metal nanoparticle instability without ligand, Ga nanodroplet coalescence, In nanodroplet coalescence, Ge nanowire chemical characterization, and error calculations (PDF)

Movie S1: Liquid TEM observation of the dissolution of clean (without surface ligands) In nanodroplets dissolving. Scale bar: 35 nm (AVI)

Movie S2: Liquid TEM observation of the coalescence of Ga microdroplets. Scale bar: $1 \mu m$ (AVI)

Movie S3: Liquid TEM observation of the coalescence of multiple ex-situ synthesized In nanodroplets. Scale bar: 15 nm (AVI)

Movie S4: Liquid TEM observation of the coalescence of in-situ synthesized In nanodroplets. Scale bar: 15 nm (AVI)

Movie S5: Liquid TEM observation of a Ge nanowire ec-LLS event from an ex-situ synthesized Ga nanodroplet. Scale bar: 100 nm (AVI)

Movie S6: Liquid TEM observation of multiple Ge nanowire ec-LLS events from in-situ synthesize nanodroplets. Scale bar: 120 nm (AVI)

Movie S7: Liquid TEM observation of an individual Ge nanowire ec-LLS event from an in-situ synthesize nanodroplet. Scale bar: 40 nm (AVI)

Movie S8: Liquid TEM observation of the volume change of in-situ synthesized In nanodroplets followed by the growth of Ge nanowires. Scale bar: 15 nm (AVI) Movie S9: Liquid TEM observation of a Ge nanowire growing under a "broad" and "focused" electron beam. Scale bar: 100 nm (AVI)

AUTHOR INFORMATION

Corresponding Author

Stephen Maldonado — Department of Chemistry and Program in Applied Physics, University of Michigan, Ann Arbor, Michigan 48109-1055, United States; orcid.org/0000-0002-2917-4851; Email: smald@umich.edu

Authors

Quintin Cheek — Department of Chemistry, University of Michigan, Ann Arbor, Michigan 48109-1055, United States Eli Fahrenkrug — Department of Chemistry, Colorado College, Colorado Springs, Colorado 80903, United States; orcid.org/0000-0002-7804-9117

Sofiya Hlynchuk – Department of Chemistry, University of Michigan, Ann Arbor, Michigan 48109-1055, United States

Daan Hein Alsem – Hummingbird Scientific, Lacey, Washington 98516, United States

Norman J. Salmon – Hummingbird Scientific, Lacey, Washington 98516, United States

Complete contact information is available at: https://pubs.acs.org/10.1021/acsnano.9b06468

Author Contributions

¹These authors contributed equally

Notes

The authors declare no competing financial interest.

ACKNOWLEDGMENTS

The authors recognize generous financial support from the National Science Foundation (CHE-1807755). The authors also acknowledge the technical support from the Michigan Center for Materials Characterization, which receives financial support from the University of Michigan College of Engineering and the National Science Foundation (DMR-9871177).

REFERENCES

- (1) Chan, C. K.; Peng, H.; Liu, G.; McIlwrath, K.; Zhang, X. F.; Huggins, R. A.; Cui, Y. High-Performance Lithium Battery Anodes Using Silicon Nanowires. *Nat. Nanotechnol.* **2008**, *3*, 31.
- (2) Garnett, E.; Yang, P. Light Trapping in Silicon Nanowire Solar Cells. *Nano Lett.* **2010**, *10*, 1082–1087.
- (3) Wang, D.; Chang, Y.-L.; Wang, Q.; Cao, J.; Farmer, D. B.; Gordon, R. G.; Dai, H. Surface Chemistry and Electrical Properties of Germanium Nanowires. *J. Am. Chem. Soc.* **2004**, *126*, 11602–11611.
- (4) Zhu, Z.; Song, Y.; Zhang, Z.; Sun, H.; Han, Y.; Li, Y.; Zhang, L.; Xue, Z.; Di, Z.; Wang, S. Vapor-Solid-Solid Grown Ge Nanowires at Integrated Circuit Compatible Temperature by Molecular Beam Epitaxy. *J. Appl. Phys.* **2017**, *122*, 094304.
- (5) Gu, J.; Collins, S. M.; Carim, A. I.; Hao, X.; Bartlett, B. M.; Maldonado, S. Template-Free Preparation of Crystalline Ge Nanowire Film Electrodes *via* an Electrochemical Liquid—Liquid—Solid Process in Water at Ambient Pressure and Temperature for Energy Storage. *Nano Lett.* **2012**, *12*, 4617—4623.
- (6) Carim, A. I.; Collins, S. M.; Foley, J. M.; Maldonado, S. Benchtop Electrochemical Liquid—Liquid—Solid Growth of Nanostructured Crystalline Germanium. *J. Am. Chem. Soc.* **2011**, *133*, 13292—13295.
- (7) Ma, L.; Lee, S.; DeMuth, J.; Maldonado, S. Direct Electrochemical Deposition of Crystalline Silicon Nanowires at T \geq 60 °C. RSC Adv. **2016**, *6*, 78818–78825.
- (8) Mahenderkar, N. K.; Liu, Y.-C.; Koza, J. A.; Switzer, J. A. Electrodeposited Germanium Nanowires. *ACS Nano* **2014**, *8*, 9524–9530.
- (9) Fahrenkrug, E.; Gu, J.; Jeon, S.; Veneman, P. A.; Goldman, R. S.; Maldonado, S. Room-Temperature Epitaxial Electrodeposition of Single-Crystalline Germanium Nanowires at the Wafer Scale from an Aqueous Solution. *Nano Lett.* **2014**, *14*, 847–852.
- (10) Seifner, M. S.; Sistani, M.; Porrati, F.; Di Prima, G.; Pertl, P.; Huth, M.; Lugstein, A.; Barth, S. Direct Synthesis of Hyperdoped Germanium Nanowires. *ACS Nano* **2018**, *12*, 1236–1241.
- (11) Acharya, S.; Ma, L.; Maldonado, S. Critical Factors in the Growth of Hyperdoped Germanium Microwires by Electrochemical Liquid–Liquid–Solid Method. *ACS Appl. Nano Mater.* **2018**, *1*, 5553–5561.
- (12) DeMuth, J.; Ma, L.; Lancaster, M.; Acharya, S.; Cheek, Q.; Maldonado, S. Eutectic-Bismuth Indium as a Growth Solvent for the Electrochemical Liquid-Liquid-Solid Deposition of Germanium Microwires and Coiled Nanowires. *Cryst. Growth Des.* **2018**, *18*, 677–685
- (13) Fahrenkrug, E.; Biehl, J.; Maldonado, S. Electrochemical Liquid—Liquid—Solid Crystal Growth of Germanium Microwires on Hard and Soft Conductive Substrates at Low Temperature in Aqueous Solution. *Chem. Mater.* **2015**, *27*, 3389—3396.
- (14) DeMuth, J.; Fahrenkrug, E.; Maldonado, S. Controlling Nucleation and Crystal Growth of Ge in a Liquid Metal Solvent. *Cryst. Growth Des.* **2016**, *16*, 7130–7138.
- (15) de Jonge, N.; Ross, F. M. Electron Microscopy of Specimens in Liquid. *Nat. Nanotechnol.* **2011**, *6*, 695.

- (16) Liao, H.-G.; Cui, L.; Whitelam, S.; Zheng, H. Real-Time Imaging of Pt₃Fe Nanorod Growth in Solution. *Science* **2012**, 336, 1011.
- (17) Zeng, Z.; Zheng, W.; Zheng, H. Visualization of Colloidal Nanocrystal Formation and Electrode–Electrolyte Interfaces in Liquids Using Tem. Acc. Chem. Res. 2017, 50, 1808–1817.
- (18) Zeng, Z.; Liang, W.-I.; Liao, H.-G.; Xin, H. L.; Chu, Y.-H.; Zheng, H. Visualization of Electrode–Electrolyte Interfaces in LiPF₆/EC/DEC Electrolyte for Lithium Ion Batteries *via In-Situ* TEM. *Nano Lett.* **2014**, *14*, 1745–1750.
- (19) Evans, J. E.; Jungjohann, K. L.; Browning, N. D.; Arslan, I. Controlled Growth of Nanoparticles from Solution with *In Situ* Liquid Transmission Electron Microscopy. *Nano Lett.* **2011**, *11*, 2809–2813.
- (20) Gu, M.; Parent, L. R.; Mehdi, B. L.; Unocic, R. R.; McDowell, M. T.; Sacci, R. L.; Xu, W.; Connell, J. G.; Xu, P.; Abellan, P.; Chen, X.; Zhang, Y.; Perea, D. E.; Evans, J. E.; Lauhon, L. J.; Zhang, J.-G.; Liu, J.; Browning, N. D.; Cui, Y.; Arslan, I.; Wang, C.-M. Demonstration of an Electrochemical Liquid Cell for Operando Transmission Electron Microscopy Observation of the Lithiation/ Delithiation Behavior of Si Nanowire Battery Anodes. *Nano Lett.* 2013, 13, 6106–6112.
- (21) Jungjohann, K. L.; Evans, J. E.; Aguiar, J. A.; Arslan, I.; Browning, N. D. Atomic-Scale Imaging and Spectroscopy for *In Situ* Liquid Scanning Transmission Electron Microscopy. *Microsc. Microanal.* **2012**, *18*, 621–627.
- (22) Liang, X.; Kim, Y.-G.; Gebergziabiher, D. K.; Stickney, J. L. Aqueous Electrodeposition of Ge Monolayers. *Langmuir* **2010**, *26*, 2877–2884.
- (23) Dickey, M. D.; Chiechi, R. C.; Larsen, R. J.; Weiss, E. A.; Weitz, D. A.; Whitesides, G. M. Eutectic Gallium-Indium (Egain): A Liquid Metal Alloy for the Formation of Stable Structures in Microchannels at Room Temperature. *Adv. Funct. Mater.* **2008**, *18*, 1097–1104.
- (24) Kattner, U. R. Phase Diagrams for Lead-Free Solder Alloys. *JOM* **2002**, *54*, 45–51.
- (25) Fahrenkrug, E.; Maldonado, S. Electrochemical Liquid—Liquid—Solid (Ec-Lls) Crystal Growth: A Low-Temperature Strategy for Covalent Semiconductor Crystal Growth. *Acc. Chem. Res.* **2015**, 48, 1881–1890.
- (26) Olesinski, R. W.; Kanani, N.; Abbaschian, G. J. The Ga-Si (Gallium-Silicon) System. *Bull. Alloy Phase Diagrams* **1985**, *6*, 362–364
- (27) Yarema, M.; Wörle, M.; Rossell, M. D.; Erni, R.; Caputo, R.; Protesescu, L.; Kravchyk, K. V.; Dirin, D. N.; Lienau, K.; von Rohr, F.; Schilling, A.; Nachtegaal, M.; Kovalenko, M. V. Monodisperse Colloidal Gallium Nanoparticles: Synthesis, Low Temperature Crystallization, Surface Plasmon Resonance and Li-Ion Storage. *J. Am. Chem. Soc.* **2014**, *136*, 12422–12430.
- (28) Gu, H.; Li, G.; Liu, C.; Yuan, F.; Han, F.; Zhang, L.; Wu, S. Considerable Knock-On Displacement of Metal Atoms under a Low Energy Electron Beam. *Sci. Rep.* **2017**, *7*, 184.
- (29) Anderson, T. J.; Ansara, I. The Ga-In (Gallium-Indium) System. J. Phase Equilib. 1991, 12, 64–72.
- (30) Zhang, J.; Zheng, Y.; Zhao, D.; Yang, S.; Yang, L.; Liu, Z.; Zhang, R.; Wang, S.; Zhang, D.; Chen, L. Ellipsometric Study on Size-Dependent Melting Point of Nanometer-Sized Indium Particles. *J. Phys. Chem. C* **2016**, *120*, 10686–10690.
- (31) Jin, B.; Sushko, M. L.; Liu, Z.; Jin, C.; Tang, R. *In Situ* Liquid Cell Tem Reveals Bridge-Induced Contact and Fusion of Au Nanocrystals in Aqueous Solution. *Nano Lett.* **2018**, *18*, 6551–6556.
- (32) Niu, K.-Y.; Liao, H.-G.; Zheng, H. Visualization of the Coalescence of Bismuth Nanoparticles. *Microsc. Microanal.* **2014**, *20*, 416–424.
- (33) Woehl, T. J.; Park, C.; Evans, J. E.; Arslan, I.; Ristenpart, W. D.; Browning, N. D. Direct Observation of Aggregative Nanoparticle Growth: Kinetic Modeling of the Size Distribution and Growth Rate. *Nano Lett.* **2014**, *14*, 373–378.

- (34) Grogan, J. M.; Schneider, N. M.; Ross, F. M.; Bau, H. H. Bubble and Pattern Formation in Liquid Induced by an Electron Beam. *Nano Lett.* **2014**, *14*, 359–364.
- (35) Zheng, H.; Smith, R. K.; Jun, Y.-w.; Kisielowski, C.; Dahmen, U.; Alivisatos, A. P. Observation of Single Colloidal Platinum Nanocrystal Growth Trajectories. *Science* **2009**, 324, 1309.
- (36) Keck, P. H.; Broder, J. The Solubility of Silicon and Germanium in Gallium and Indium. *Phys. Rev.* **1953**, *90*, 521–522.
- (37) Olesinski, R. W.; Abbaschian, G. J. The Ga-Ge (Gallium-Germanium) System. Bull. Alloy Phase Diagrams 1985, 6, 258–262.
- (38) Chen, W.; Yu, L.; Misra, S.; Fan, Z.; Pareige, P.; Patriarche, G.; Bouchoule, S.; Cabarrocas, P. R. i. Incorporation and Redistribution of Impurities into Silicon Nanowires During Metal-Particle-Assisted Growth. *Nat. Commun.* **2014**, *5*, 4134.
- (39) Heitsch, A. T.; Fanfair, D. D.; Tuan, H.-Y.; Korgel, B. A. Solution-Liquid-Solid (Sls) Growth of Silicon Nanowires. *J. Am. Chem. Soc.* **2008**, *130*, 5436–5437.
- (40) Wang, F.; Dong, A.; Buhro, W. E. Solution—Liquid—Solid Synthesis, Properties, and Applications of One-Dimensional Colloidal Semiconductor Nanorods and Nanowires. *Chem. Rev. (Washington, DC, U. S.)* **2016**, *116*, 10888—10933.
- (41) Noh, K. W.; Liu, Y.; Sun, L.; Dillon, S. J. Challenges Associated with *In-Situ* Tem in Environmental Systems: The Case of Silver in Aqueous Solutions. *Ultramicroscopy* **2012**, *116*, 34–38.
- (42) Park, J. H.; Schneider, N. M.; Grogan, J. M.; Reuter, M. C.; Bau, H. H.; Kodambaka, S.; Ross, F. M. Control of Electron Beam-Induced Au Nanocrystal Growth Kinetics through Solution Chemistry. *Nano Lett.* **2015**, *15*, 5314–5320.
- (43) Woehl, T. J.; Evans, J. E.; Arslan, I.; Ristenpart, W. D.; Browning, N. D. Direct *In Situ* Determination of the Mechanisms Controlling Nanoparticle Nucleation and Growth. *ACS Nano* **2012**, *6*, 8599–8610.
- (44) Bresin, M.; Chamberlain, A.; Donev, E. U.; Samantaray, C. B.; Schardien, G. S.; Hastings, J. T. Electron-Beam-Induced Deposition of Bimetallic Nanostructures from Bulk Liquids. *Angew. Chem.* **2013**, 125. 8162–8165.
- (45) Woehl, T. J.; Abellan, P. Defining the Radiation Chemistry During Liquid Cell Electron Microscopy to Enable Visualization of Nanomaterial Growth and Degradation Dynamics. *J. Microsc.* **2017**, 265, 135–147.
- (46) Kallesøe, C.; Wen, C.-Y.; Booth, T. J.; Hansen, O.; Bøggild, P.; Ross, F. M.; Mølhave, K. *In Situ* Tem Creation and Electrical Characterization of Nanowire Devices. *Nano Lett.* **2012**, *12*, 2965–2970
- (47) Kallesøe, C.; Wen, C.-Y.; Mølhave, K.; Bøggild, P.; Ross, F. M. Measurement of Local Si-Nanowire Growth Kinetics Using *In Situ* Transmission Electron Microscopy of Heated Cantilevers. *Small* **2010**, *6*, 2058–2064.
- (48) Kodambaka, S.; Hannon, J. B.; Tromp, R. M.; Ross, F. M. Control of Si Nanowire Growth by Oxygen. *Nano Lett.* **2006**, *6*, 1292–1296.
- (49) Wu, Y.; Yang, P. Direct Observation of Vapor-Liquid-Solid Nanowire Growth. J. Am. Chem. Soc. 2001, 123, 3165-3166.
- (50) Chockla, A. M.; Korgel, B. A. Seeded Germanium Nanowire Synthesis in Solution. *J. Mater. Chem.* **2009**, *19*, 996–1001.
- (51) Fahrenkrug, E.; Alsem, D. H.; Salmon, N.; Maldonado, S. Electrochemical Measurements in *In Situ* Tem Experiments. *J. Electrochem. Soc.* **2017**, *164*, H358–H364.
- (52) Ross, F. M.; Liquid Cell Electron Microscopy; Cambridge University Press: Cambridge, 2016.
- (53) Francis, Z.; Incerti, S.; Karamitros, M.; Tran, H. N.; Villagrasa, C. Stopping Power and Ranges of Electrons, Protons and Alpha Particles in Liquid Water Using the Geant4-DNA Package. *Nucl. Instrum. Methods Phys. Res., Sect. B* **2011**, 269, 2307–2311.
- (54) Meesungnoen, J.; Jay-Gerin, J.-P.; Filali-Mouhim, A.; Mankhetkorn, S. Low-Energy Electron Penetration Range in Liquid Water. *Radiat. Res.* **2002**, *158*, 657–660.

- (55) Gupta, T.; Schneider, N. M.; Park, J. H.; Steingart, D.; Ross, F. M. Spatially Dependent Dose Rate in Liquid Cell Transmission Electron Microscopy. *Nanoscale* **2018**, *10*, 7702–7710.
- (56) Newbury, D. E.; Joy, D. C.; Goldstein, J. I.; Ritchie, N. W. M.; Scott, J. H. J.; Michael, J. R. Scanning Electron Microscopy and X-Ray Microanalysis, 4th ed.; Springer: New York, 2017.
- (57) Zhang, T.; Fahrenkrug, E.; Maldonado, S. Electrochemical Liquid-Liquid-Solid Deposition of Ge at Hg Microdroplet Ultramicroelectrodes. *J. Electrochem. Soc.* **2016**, *163*, D500–D505.
- (58) Kashchiev, D. Dependence of the Growth Rate of Nanowires on the Nanowire Diameter. Cryst. Growth Des. 2006, 6, 1154–1156.
- (59) Weyher, J. Some Notes on the Growth Kinetics and Morphology of VLS Silicon Crystals Grown with Platinum and Gold as Liquid-Forming Agents. *J. Cryst. Growth* **1978**, 43, 235–244.
- (60) Nebol'sin, V. A.; Shchetinin, A. A.; Dolgachev, A. A.; Korneeva, V. V. Effect of the Nature of the Metal Solvent on the Vapor-Liquid-Solid Growth Rate of Silicon Whiskers. *Inorg. Mater.* **2005**, *41*, 1256–1259
- (61) Shakthivel, D.; Raghavan, S. Vapor-Liquid-Solid Growth of Si Nanowires: A Kinetic Analysis. *J. Appl. Phys.* **2012**, *112*, 024317.
- (62) Dubrovskii, V. G.; Sibirev, N. General Form of the Dependences of Nanowire Growth Rate on the Nanowire Radius. *J. Cryst. Growth* **2007**, *304*, 504–513.
- (63) Li, N.; Li, W.; Liu, L.; Tan, T. Y. A Nucleation-Growth Model of Nanowires Produced by the Vapor-Liquid-Solid Process. *J. Appl. Phys.* **2013**, *114*, 064302.
- (64) Schmidt, V.; Senz, S.; Gosele, U. Diameter Dependence of the Growth Velocity of Silicon Nanowires Synthesized *via* the Vapor-Liquid-Solid Mechanism. *Phys. Rev. B: Condens. Matter Mater. Phys.* **2007**, 75, 045335.
- (65) Schubert, L.; Werner, P.; Zakharov, N. D.; Gerth, G.; Kolb, F. M.; Long, L.; Gösele, U.; Tan, T. Y. Silicon Nanowhiskers Grown on (111) Si Substrates by Molecular-Beam Epitaxy. *Appl. Phys. Lett.* **2004**, *84*, 4968–4970.
- (66) Rudolph, P. Fundamentals of Defects in Crystals. AIP Conf. Proc. 2007, 916, 69–92.
- (67) Belloni, J. Nucleation, Growth and Properties of Nanoclusters Studied by Radiation Chemistry: Application to Catalysis. *Catal. Today* **2006**, *113*, 141–156.
- (68) Rojas, J. V.; Castano, C. H. Radiolytic Synthesis of Iridium Nanoparticles onto Carbon Nanotubes. *J. Nanopart. Res.* **2014**, *16*, 2567.
- (69) Kind, C.; Feldmann, C. One-Pot Synthesis of InO Nanoparticles with Tuned Particle Size and High Oxidation Stability. *Chem. Mater.* **2011**, 23, 4982–4987.